ELSEVIER

NDT&E International 34 (2001) 239–248

NDT&E international

www.elsevier.com/locate/ndteint

Micro-damage diagnostics using nonlinear elastic wave spectroscopy (NEWS)

Koen E-A. Van Den Abeele[a,*], Alexander Sutin[b], Jan Carmeliet[c], Paul A. Johnson[d]

[a]*Interdisciplinary Research Center, Catholic University Leuven, Campus Kortrijk, B-8500 Kortrijk, Belgium*
[b]*Stevens Institute of Technology, Hoboken, NJ 07030, USA*
[c]*Department of Building Physics, Catholic University Leuven, B-3001 Heverlee, Belgium*
[d]*Los Alamos National Laboratory, Los Alamos, NM 87545, USA*

Abstract

Nonlinear elastic wave spectroscopy (NEWS) represents a class of powerful tools which explore the dynamic nonlinear stress–strain features in the compliant bond system of a micro-inhomogeneous material and link them to micro-scale damage. Hysteresis and nonlinearity in the constitutive relation (at the micro-strain level) result in acoustic and ultrasonic wave distortion, which gives rise to changes in the resonance frequencies as a function of drive amplitude, generation of accompanying harmonics, nonlinear attenuation, and multiplication of waves of different frequencies. The sensitivity of nonlinear methods to the detection of damage features (cracks, flaws, etc.) is far greater than can be obtained with linear acoustical methods (measures of wavespeed and wave dissipation). We illustrate two recently developed NEWS methods, and compare the results for both techniques on roofing tiles used in building construction.

Keywords: Nonlinear acoustics; Nonlinearity; Hysteresis; Damage diagnostics

1. Introduction

In recent years, the study of dynamic nonlinearity and hysteresis in micro-inhomogeneous media has experienced an impressive growth. Even though the complex dynamic nonlinear stress–strain features at the mesoscale level are not yet completely understood and/or agreed upon, this area of research has led to a prominent set of applications in the field of non-destructive damage diagnostics. Experimental evidence demonstrates that the nonlinear elasticity of a piece of metal, composite or plexiglass increases dramatically when it becomes damaged, displaying nonlinear mesoscopic behaviour that appears to be much like that in rock or concrete [1–6]. Various techniques have been developed in order to quantify the level of nonlinearity in the elastic response of materials containing structural inhomogeneity and damage. We have termed this class of techniques Nonlinear Elastic Wave Spectroscopy, or shortened NEWS. Traditionally, wave propagation techniques were used to probe the generation of the second harmonic frequency component as function of distance or amplitude [7–13]. Other techniques include quasi-static time-of-flight measurements (as function of the applied external pressure) [4,14,15], modulation experiments by frequency mixing [5,16–19], studies of the amplitude dependence of the resonance spectrum [6,20–23], reverberation measurements at various excitation amplitudes [23], and investigations of slow dynamic behaviour [24–26]. As a general conclusion, it was found that the nonlinear methods are much more sensitive to the damage-related structural alterations than any other method based on the investigation of the linear material parameters such as wavespeed and damping.

In this paper, we report on two NEWS approaches and their application to monitor progressive micro-damage detection in materials. The first NEWS method, Single Mode Nonlinear Resonant Acoustic Spectroscopy (SIMONRAS), involves a study of the nonlinear response of a single resonant mode of a material's specimen [6,20–23]. Resonance frequency shifts, harmonics and damping characteristics are analysed as function of the resonance peak acceleration or strain amplitude. The second method presented here is Nonlinear Wave Modulation Spectroscopy (NWMS), which consists of exciting a sample with signals pertaining to two separate frequency bands simultaneously, and inspecting the harmonics of the two waves, and their sum and difference frequencies (sidebands) [5,16–19].

* Corresponding author. Tel.: +32-56-246-256; fax: +32-56-246-999.
E-mail address: koen.vandenabeele@kulak.ac.be (K.E-A. Van Den Abeele).

0963-8695/01/$ - see front matter
PII: S0963-8695(00)00064-5

Undamaged materials are essentially linear in their response, while the same material, when damaged, becomes highly nonlinear, manifested by a significant resonance frequency shift with amplitude, nonlinear attenuation, and harmonics and sideband generation. We will illustrate the methods by experiments on intact and damaged building construction and industrial components. A comparison of both techniques on slate roofing tiles shows evidence for the robustness of the different nonlinear measurements in relation to damage. As in the case of any global diagnostic method, a complementary example shows that scaling is an important issue. The density of cracks and mesoscopic inhomogeneities highly influences the sensitivity of the techniques.

In order to comprehend the analysis of the experimental data, we first briefly review the current state of the art in dynamic modelling of nonlinear elasticity and acoustic wave interaction in materials with large nonlinearity and hysteresis.

2. State of the art in modelling nonlinearity and hysteresis

The huge nonlinear response of micro-inhomogeneous and damaged materials arises from the complex compliance of local or volumetric cracks and features (pores, contacts, etc.) in the bond system between the constituents. At a mesoscopic level, the local nonlinear forces in the bond system may entirely dominate the relatively small classical (atomic) nonlinearity of the rigid units surrounding them. Even though the full mechanism of the nonlinear response is not yet completely understood, there is a strong consensus that most micro-inhomogeneous materials exhibit hysteresis and discrete memory in their stress–strain relation, even at a low to moderate strain level [27–33]. Following the phenomenological description of stress–strain hysteresis in rocks by Guyer and McCall [28–30], the 1D constitutive relation between the stress σ and the strain ϵ can be expressed in a first approximation as follows:

$$\sigma = \int K(\epsilon, \dot{\epsilon})\, \mathrm{d}\epsilon \tag{1a}$$

with K the strain amplitude and strain rate dependent modulus given by

$$K(\epsilon(t), \dot{\epsilon}(t)) = K_0(1 - \beta\epsilon(t) - \delta\epsilon(t)^2 - \alpha(\Delta\epsilon + \epsilon(t) \times \mathrm{sign}(\dot{\epsilon}(t))) + \ldots) \tag{1b}$$

where K_0 is the linear modulus, $\Delta\epsilon$ is the local strain amplitude over the previous period ($\Delta\epsilon = (\epsilon_{\mathrm{Max}} - \epsilon_{\mathrm{Min}})/2$ for a simple continuous sine excitation), $\dot{\epsilon} = \mathrm{d}\epsilon/\mathrm{d}t$ the strain rate, $\mathrm{sign}(\dot{\epsilon}) = 1$ if $\dot{\epsilon} > 0$ and $\mathrm{sign}(\dot{\epsilon}) = -1$ if $\dot{\epsilon} < 0$ [28–30,32,33]. The parameters β and δ are the classical nonlinear perturbation coefficients in the Taylor expansion of stress versus strain [34–36]; α is introduced as a measure of the material hysteresis.

The formulation of the nonlinear modulus in Eq. (1b) has several interesting implications on the acoustic wave propagation, which clearly differentiate between a classical nonlinear and a hysteretic nonlinear behaviour. In a classical nonlinear system, a strain wave of frequency f and amplitude $\Delta\epsilon$ can transform into a strain wave with frequency components $2f$, $3f$, etc. for which the amplitudes are proportional to $(\Delta\epsilon)^2$, $(\Delta\epsilon)^3$, etc. In the case of a purely hysteretic material, the second harmonic cannot be generated, and the third harmonic is found to be quadratic in the fundamental strain amplitude [28,30–33]. This implies that hysteresis acts as a second order nonlinearity. Analogously, in a modulation experiment involving frequencies f_1 and f_2 with amplitudes $\Delta\epsilon_1$ and $\Delta\epsilon_2$, the first order intermodulation frequencies at $f_2 \pm f_1$ arise from the classical two-fold nonlinear interaction between f_1 and f_2, and their amplitude is proportional to $\beta \times \Delta\epsilon_1 \times \Delta\epsilon_2$. When dynamic hysteresis prevails, the second order sidebands ($f_2 \pm 2f_1$) will display amplitudes proportional to $\alpha \times \Delta\epsilon_1 \times \Delta\epsilon_2$, whereas classical theory would predict a higher order dependence: $C_{\beta\delta}(\Delta\epsilon_1)^2 \times \Delta\epsilon_2$, with $C_{\beta\delta}$ a linear combination of β^2 and δ.

When we apply the phenomenological formulation to the modelling of resonant-wave experiments, and substitute Eq. (1a) into a lumped element equation [21,25], the nonlinear contribution to the solution gives rise to a decrease of the resonance frequency which is in first approximation proportional to the peak strain amplitude $\Delta\epsilon$ in the resonance curve:

$$\frac{f_0 - f}{f_0} = C_1\Delta\epsilon + \text{higher order.} \tag{2}$$

In addition, a quadratic amplitude dependence of the third harmonic is predicted:

$$\Delta\epsilon_{3f} = C_2\Delta\epsilon^2 + \text{higher order.} \tag{3}$$

together with a linear increase of the attenuation or modal damping ratio (MDR):

$$\frac{\xi - \xi_0}{\xi_0} = C_3\Delta\epsilon + \text{higher order.} \tag{4}$$

Here, f is the resonance frequency at strain amplitude $\Delta\epsilon$, f_0 is the linear (or low amplitude) resonance frequency. Analogously, ξ is the MDR at strain amplitude $\Delta\epsilon$, ξ_0 is the linear (or low amplitude) MDR. The coefficients C_i in all three relationships are proportional to the hysteresis parameter α. Any increase in the measured values of these coefficients reflects an increase of the nonlinear hysteresis behaviour of the material. Finally, in agreement with wave propagation experiments, it can be shown that the presence of hysteresis does not affect the level of the even harmonics in resonance [21,32].

As in the case of wave propagation and wave modulation, it is important to note that these results are fundamentally

different from a classical approach in which a nonlinear oscillator, such as the Duffing type oscillator, is described [37]. A classical treatment of nonlinear oscillations, using a power law expansion of the constitutive equation, predicts a first order quadratic decrease of the resonance frequency with increasing drive voltage, together with a cubic amplitude dependence of the third harmonic amplitude. Furthermore, there will be no nonlinear energy dissipation in a classical system.

In the next section, we will describe and analyse nonlinear resonance and wave modulation experiments within the framework of non-classical nonlinear modelling.

3. NEWS techniques

Nonlinear spectroscopic techniques principally intend to monitor the amplitude dependent response of materials, which can in turn be associated to characteristic parameters describing the nonlinear behaviour of material properties such as the Young's modulus, the MDR, etc. In this paper we restrict ourselves to the following two techniques: SIMONRAS and NWMS. We illustrate both techniques with an example and show the qualitative and semi-quantitative agreement of both methods on roofing tiles.

3.1. Configuration and example of SIMONRAS

SIMONRAS involves a study of the nonlinear response of a single resonant mode of the material specimen. Resonance frequency shifts, and harmonics and damping characteristics are analysed as function of the resonance peak acceleration amplitude.

A detailed discussion of the experimental apparatus can be found in several previously published papers by the Nonlinear Elasticity group of Los Alamos National Laboratory in collaboration with various European Institutes and Universities [6,20–23]. At the Laboratory of Building Physics of the Catholic University of Leuven, Belgium, the SIMONRAS technique was adopted and applied to characterise and assess damage in various building materials [6,22,23]. As an example, we consider a thin, rectangular beam ($400 \times 26 \times 4$ mm^3) of fibre-cemented (artificial) slate used in roofing constructions. The synthetic fibres (4 mm in length, a few tens of microns in diameter) used in the production process have a principal orientation perpendicular to the length-wise direction of the beam. The beam is excited at its lowest order flexural (bending) resonance mode by a low frequency, low distortion speaker, positioned at 2 cm from the middle, parallel to the beam surface. The sample is suspended with nylon wires at the nodal lines of the considered mode. The coupling medium between specimen and speaker is air (non-contact excitation). The speaker is driven in discrete frequency steps by a function generator through a high power amplifier. The sample's out of plane response is recorded by an accelerometer and postprocessed using LabVIEW. In order to monitor resonant peak shift and harmonic generation, 4–10 resonance (discrete) sweeps over the same frequency interval, encompassing the first flexural mode, are made at successively increasing drive voltages. The procedure is completely computer controlled.

Let us first consider a sample that is virtually intact. Fig. 1a illustrates that the resonance curves scale close to linearly with the measured amplitude. Plotting the relative resonance frequency shift, $(f_0 - f)/f_0$, versus the peak strain, reveals a slight decrease of the resonance frequency f proportional with the increasing strain amplitude (Fig. 1b). The measured harmonics, obtained at peak resonance, are all at least 60 dB below the fundamental (Fig. 1c). The attenuation factor (expressed in terms of the MDR, ξ [38]) is barely increasing with amplitude ($(\xi - \xi_0)/\xi_0$ is plotted in Fig. 1d for increasing peak resonance strain amplitude). The proportional decrease of the resonance frequency and the increase of MDR are in agreement with the nonlinear hysteresis model discussed in the previous section. Fitting the first order relations (Eqs. (2)–(4)) to the data, we obtain a value of 30 for C_1, and 1600 for C_3. Compared to rock-type materials, these values are about two orders of magnitude smaller.

For a damaged sample (actually, the above described intact beam after several hydrothermal shocks), the nonlinear softening becomes significantly more apparent. A similar analysis of the resonance frequency shows that the nonlinear effect is raised by two orders of magnitude due to the hydrothermally induced microdamage (Fig. 2). The amplitude dependence is still linear (Fig. 2b). Also, with the larger frequency shift, the harmonic spectrum changes dramatically (Fig. 2c). The third harmonic becomes dominant, and its dependence on the fundamental acceleration amplitude is basically quadratic. Note that the second harmonic does not nearly show a similar increase (in the intact case the level of the second and third harmonic were equal). Also, the fifth harmonic has increased significantly in comparison with the fourth harmonic. Finally, we observe a significant increase in nonlinearity of the damping (Fig. 2d). The attenuation depends linearly on the measured resonance amplitude (for a method to invert the attenuation in the case of a skewed resonance peak, we refer the reader to the work of Smith and TenCate [39]). The value of C_3 has increased by a factor 200, which is in good agreement with the relative increase of the factor C_1. The increase of the third harmonic dependence is roughly of the same order. The linear wavespeed (or equivalent, the low amplitude resonance frequency) of the intact versus the damaged specimen only changed by 7.6% and the linear attenuation value increased with 66%. Careful inspection using X-ray radiography revealed several uniformly distributed hairline cracks perpendicular to the length-wise direction of the beam (i.e. parallel to the orientation of the fibres). These cracks were not visible with bare eye.

The observed relationships between the drive amplitudes and the various nonlinear phenomena (resonant frequency shift or modulus reduction, attenuation increase and third

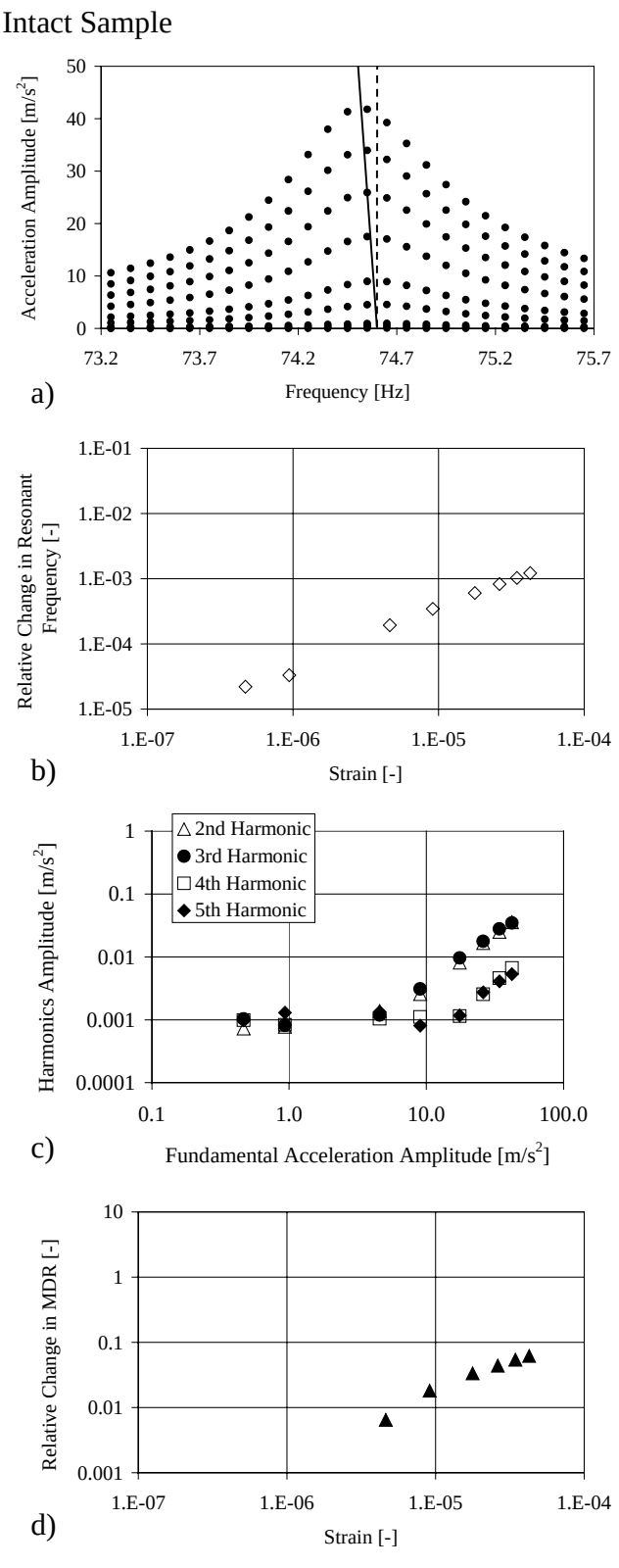

Fig. 1. SIMONRAS results obtained on the first bending mode of an intact slate beam: (a) measured resonance curves at eight different drive levels; (b) relative resonant frequency shift as function of the peak strain amplitude measured at the different drive levels; (c) harmonic content at peak acceleration; (d) relative change of the measured attenuation as function of peak strain.

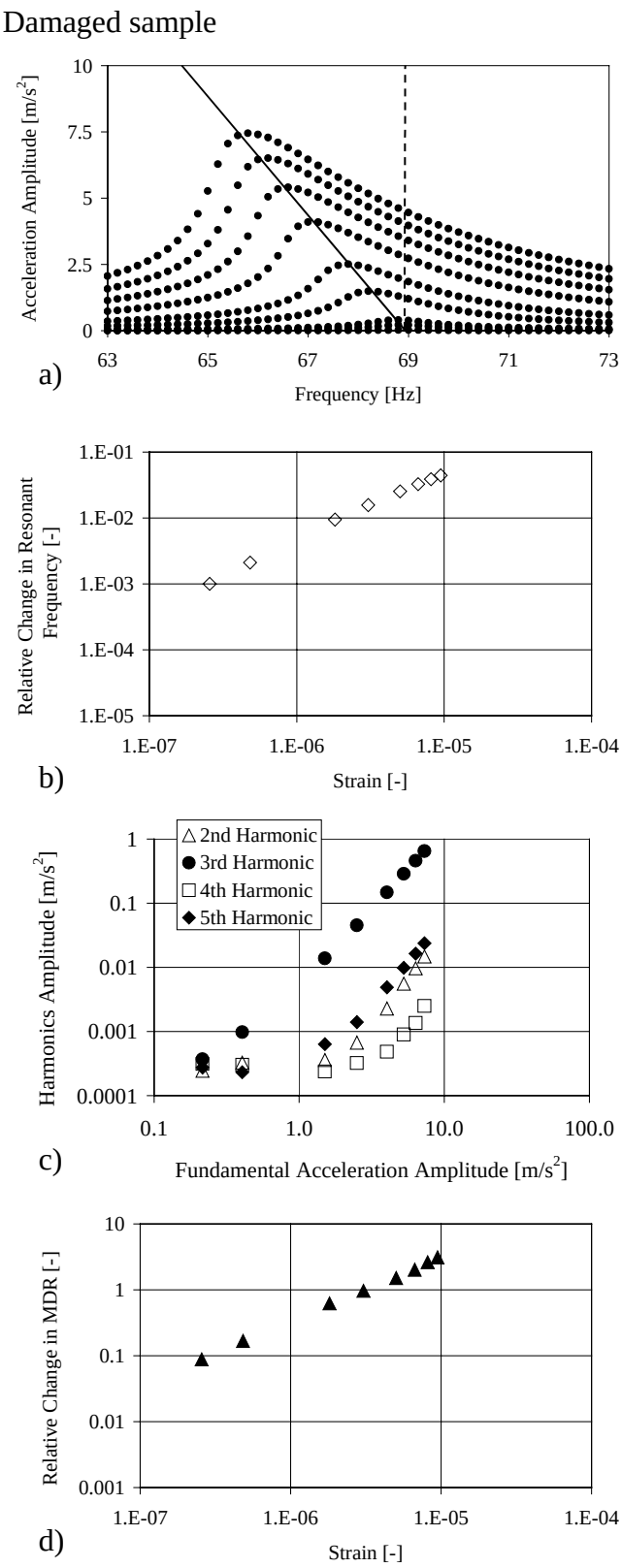

Fig. 2. SIMONRAS results obtained on the first bending mode of a micro-damaged slate beam. Similar division in subfigures as in Fig. 1.

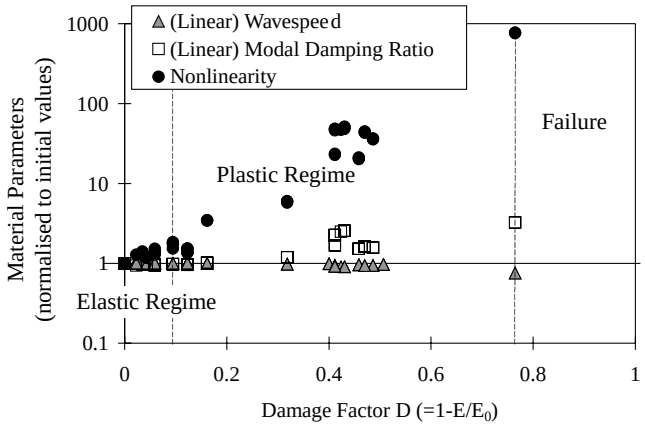

Fig. 3. Variation of two linear material parameters and of the nonlinear parameter C_1 with respect to their initial values during a cyclic fatigue loading experiment (three-point bending).

harmonic generation) clearly imply that the type of nonlinearity of the material is dominated by dynamic hysteresis in the stress–strain behaviour. Since the experimental set-up was identical in the intact and the damaged case, the increase of the nonlinear effects is solely caused by microcracking and damage induced by the hydrothermal shocks. Consequently, in order to quantify the level of damage, it suffices to determine the value of C_1 (or C_2 or C_3) of a sample relative to the initial state (intact specimen) of the material.

The characterisation procedure has also been applied to damage detection in thin slate beams subjected to cyclic fatigue loading. After each loading session, the linear (wavespeed and wave dissipation) and nonlinear parameters (C_1) were measured. At the same time, the apparent instantaneous static modulus, E, is determined from the quasi-static force-displacement curves. This value allows us to introduce a 'local' stiffness degradation parameter or damage factor D, defined as $D = 1 - E/E_0$, with E_0 the initial stiffness value of the beams. In the elastic regime, there is almost no reduction of the static Young's modulus: $D \cong 0.0$. In the plastic regime, the modulus is continuously softening: $0.0 < D < 0.5$. Finally, the modulus decreases quickly and drastically in the terminal regime: $D > 0.5$. Fig. 3 summarises the evolution of the linear and nonlinear parameters relative to their initial values (on a logarithmic scale!) as the value of D increases. The sensitivity of the nonlinear method to the apparent stiffness reduction (due to the development of microcracks, flaws, etc.) is far greater than in the case of the linear acoustical methods. At failure the nonlinearity increased by a factor 1000, whereas the linear (low amplitude) attenuation only increased by a factor of 5 and the linear resonance frequency (or wavespeed) reduced by 25%. An X-ray micrograph of the damaged zone just before failure is shown in Fig. 4.

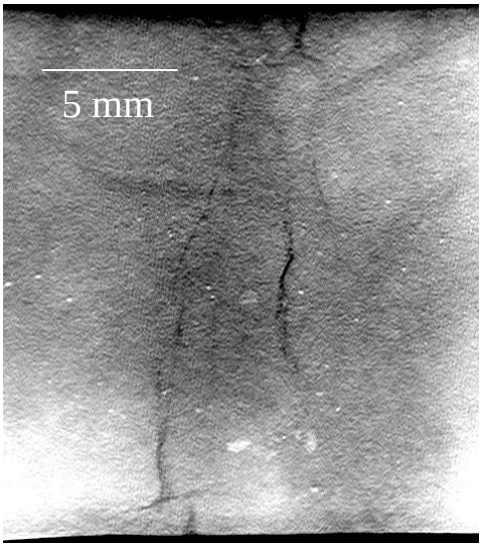

Fig. 4. X-ray radiography of the damaged zone in a thin strip of artificial slate. Just before failure, microcracks coalesce to form a macrocrack visible from the surface.

3.2. Configuration and example of NWMS

NWMS consists of simultaneously exciting a sample with two autonomous waves, which frequency spectra are confined to two separate ranges, and inspecting the harmonics in the material's response to the two waves. We pay particular attention to the sum and difference frequencies (sidebands).

NWMS can be applied in continuous mode or in impact mode [5,16–19]. In continuous mode, two sinusoidal waves with separate frequencies are input into the sample simultaneously using speakers or piezoelectric transducers. The first speaker or transducer generates a low frequency signal, whereas the second one produces a high frequency wave. The response is recorded at a separate location on the sample. The waveform is Fourier analysed and the interaction of the two input signals is investigated. In a sample that is intact, the output spectrum contains the two frequencies that have been affected by linear processes of wave dissipation and scattering, and by small atomic nonlinearities. In a sample that is damaged, harmonics and sidebands are created by the nonlinearity of the medium in addition to the linear effects. The presence of the harmonics and sidebands indicates microcracking and damage.

In impact mode the sample is excited by tapping it with an impact hammer, while a high frequency continuous signal generated by a separate speaker/transducer is propagating through the sample. The use of an impact signal as a low frequency component is particularly interesting and advantageous because it efficiently excites the entire resonance mode spectrum of the sample at once. Again, the interaction between the impact signal and the high frequency wave can be quantified and used in the assessment of damage within the sample. This method can be quickly applied, and in our view, is ideally suited to applications where the question of damaged versus undamaged must be quickly addressed.

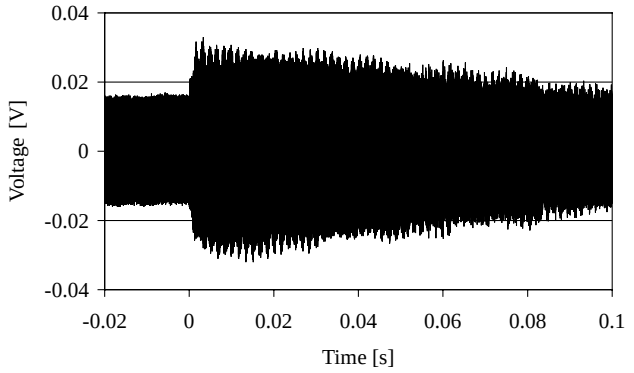

Fig. 5. Typical time series acquired in an application of NWMS to differentiate intact and damaged automobile components.

We illustrate the NWMS-impact mode with an application of microcrack detection on automobile engine connecting rods, which have a complex geometry much like an elongated number eight. The spectrum of such components corresponding to the hammer impact is limited in frequency band to about 20 kHz because of the size of the specimen and the attenuation of the material. In addition, the low frequency signal generated by the impact only persists for a limited time, and is attenuated with a characteristic decay time, which is of the order of 50–100 ms. The high frequency signal is generated by a piezo-ceramic transducer attached to the sample, and fixed at 127 kHz with a constant voltage. A typical example of an acquired time signal triggered at 20 ms before the impact is shown in Fig. 5. In order to analyse the nonlinear (or amplitude dependent) behaviour of the samples, we applied a moving time window analysis to the measured signal. Each time window was 10 ms long and contained 4000 data points. For each of these intervals a spectral analysis was performed. The modulation spectra are illustrated in Fig. 6 as a contour plot (darker colours represent higher intensity). In each subfigure, each vertical line corresponds to the modulation spectrum for a given time window. The bottom line represents the spectrum of the first window after triggering the impact, the top line is the spectrum of the last possible time window. Even though energy is abundantly present in the low frequency band, there is no interaction with the high frequency component for the intact automobile component (see blow-up on top subfigure). On the other hand, an identical sample with a tiny crack in the connecting arm shows large levels of energy in the sidebands (second blow-up). Subsequent to the Fourier analysis of each window, each power spectrum is integrated over two limited spectral bands, yielding the 'equivalent energy' values EE_1 and EE_2 for the low (0–20 kHz) and the high frequency (120–134 kHz), respectively. After subtraction of the 'energy' contained in the high frequency component from EE_2, we plot the resulting value ('the sideband energy') against EE_1 ('impact energy'). The outcome of this procedure applied to ten equally spaced time windows is shown in Fig. 7 for the intact as well as the damaged sample, showing the sideband energy versus the impact energy. For the intact unit, we observe a modest increase of the sideband energy proportional to the impact energy. In the case of the damaged unit, the dependence is also close to linear, but it is far more manifest. The proportionality coefficient of this linear relationship may be used as a damage indicator in quality control, and may be integrated in a production line.

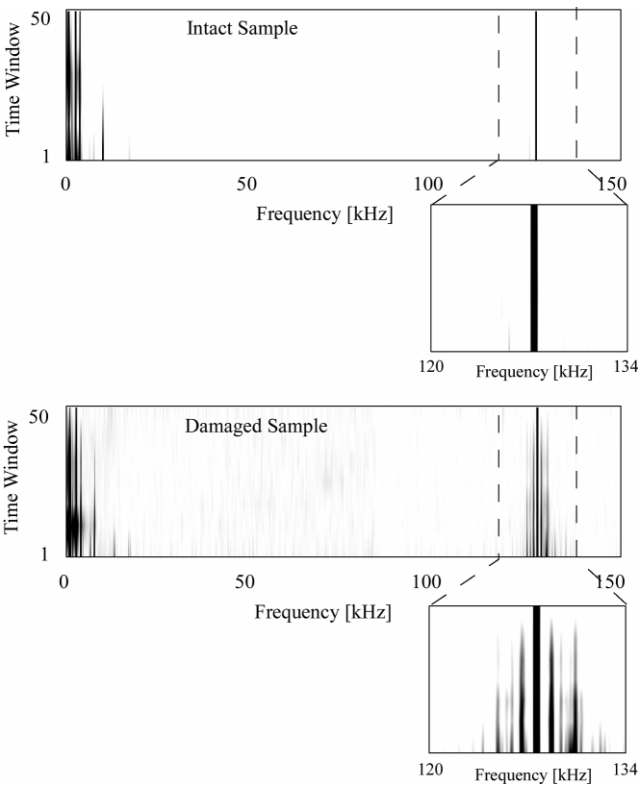

Fig. 6. Contour plots of the modulation spectra in NWMS-impact mode for an intact and a damaged automobile component. The high frequency band is enlarged to show the extreme sidelobe generation in the case of a damaged sample.

3.3. Comparison of SIMONRAS and NWMS on cementitious roofing tiles

As a follow-up to the investigation of progressive damage in thin slate strips, we applied both SIMONRAS and NWMS to industrial production plates of fibre-cemented slate used in roofing construction (nominal dimensions are $400 \times 600 \times 4$ mm^3). The aim of this investigation was to find an operator independent measure of the severity of edgecracking, which occurs during and after the production process. Edgecracks originate during drying or cutting of the samples, and may have an unfavourable influence on the lifetime of the material.

Because of the different geometry and the location of the cracks, the plate problem was studied by examining the eighth natural mode of the structure. Apart from being well isolated from other resonances, this mode has six relatively broad locations of maximum stress near the edges

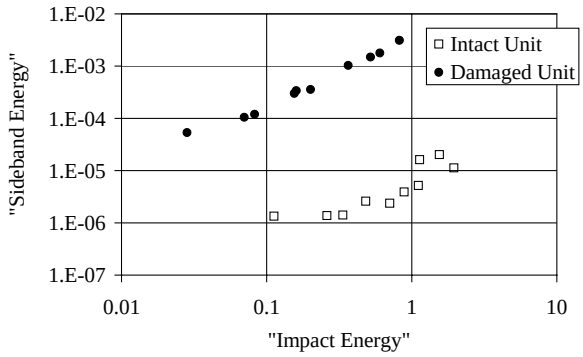

Fig. 7. Integration analysis of the wave modulation spectra for an intact and a cracked engine part in NWMS-impact mode illustrating the amount of 'sideband energy' in relation to the 'impact energy' for consecutive time windows after impact.

(two on each long side, one on each short side) and is therefore a good candidate to detect edgecracks. A similar set-up as for the rectangular strips of slate was used to perform SIMONRAS on a batch of 60 plates. The SIMONRAS measurements were quantified in terms of the nonlinearity parameter C_1', which can be inferred from the frequency shift proportionality to the acceleration amplitude (Eq. (2), replacing strain by acceleration: $\Delta f/f_0 = C_1' \times \mathrm{Acc}$). Since all plates have virtually the same geometry, composition and stiffness, we may assume that the value of C_1' is uniformly proportional to the dimensionless value C_1. Likewise C_3' was determined from the nonlinear attenuation data using Eq. (4) in terms of the acceleration amplitude. Fig. 8 clearly shows a 'one-to-one' relation between the two SIMONRAS nonlinearity parameters, indicating that they originate from the same nonlinear mechanism, namely dynamic hysteresis in the stress–strain relation.

In order to check the independence of the results to the nonlinear method used, we selected five plates and performed NWMS measurements on these specimen using the impact mode. The use of a broadband low frequency signal guarantees that several platemodes are excited at once, including the resonances with stress

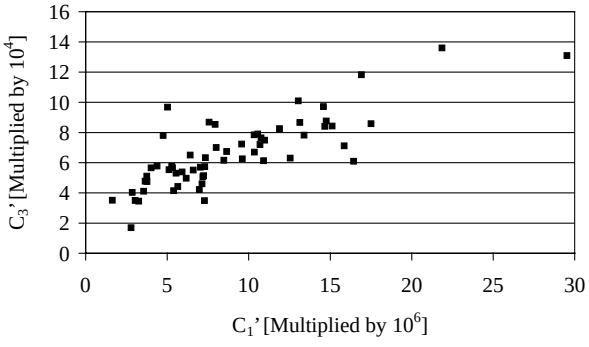

Fig. 8. Results of a SIMONRAS analysis on a batch of 60 fibre-cemented plates, showing a good correlation between the nonlinearity parameter C_3', deduced from the nonlinear attenuation, and the nonlinearity parameter C_1', deduced from the resonant frequency shift.

concentrations near the plate boundaries which are activating the edge-cracks. Among the selected specimen, two plates had a low SIMONRAS C_1' value (8×10^{-6}), two a medium value (15×10^{-6}) and the fifth plate had a large value (22×10^{-6}). For each plate, 11 NWMS measurements were performed which probe the modulation of a transient impact with a high frequency component at consecutive frequencies ranging from 140 to 150 kHz. The 11 Fourier spectra are renormalised with respect to the high frequency component, and averaged. In addition, the sideband energy is calculated by integrating the averaged spectrum and subtracting the central component. The results for each plate are summarised in Fig. 9. The comparison of the value of the sideband energy with the SIMONRAS parameter for nonlinearity shows a convincing linear relationship (Fig. 10), which implies that the nonlinear measurements of both methods are highly consistent.

3.4. Investigation of crackdensity and location on the sensitivity of global nonlinear techniques

In a subsequent study, the values of the SIMONRAS nonlinearity for a batch of 60 slate plates were compared to the results of a visual inspection method, which consists of wetting the sample and counting the edgecracks as water imbibes under bending tension. Unfortunately, the correlation between the nonlinear measurements and the crack-counts from the visual inspection turned out to be poor. Several plates with a large nonlinearity parameter showed only a small number of cracks and vice versa. In order to investigate this discrepancy in more detail, we selected three plates for further examination: one reference plate (R) with a small number of cracks (7) and a small coefficient of nonlinearity ($C_1' = 5 \times 10^{-6}$) and two (hydrothermally shocked) plates (P_1 and P_2) with a large number of cracks (48 and 47), but with a widely different nonlinear coefficient ($C_1' = 14 \times 10^{-6}$ and $C_1' = 26 \times 10^{-6}$, respectively). The location of the edgecracks as indicated after visual inspection are shown in Fig. 11. Next, the plates were water-sawed into 19 strips of $25 \times 400 \times 4$ mm^3 (13 length-wise and six lateral, as indicated in Fig. 11) and dried for a period of time. Subsequently, the nonlinearity of each strip was determined by means of a SIMONRAS experiment on the 1st bending mode. The results for the strips, plotted as a function of position in the original plate, are shown on the bottom row of Fig. 11. In order to eliminate the influence of the drying time between different plates, we took the ratio of the nonlinear coefficient of each strip to the average of the five central pieces in the same plate. We note a dramatic increase in nonlinearity of the edge-strips of the two cracked plates. The nonlinearity in the centre of both plates is nearly constant and increases abruptly by a factor of 50 for the outermost length-wise pieces where the density of the cracks is largest. The difference between

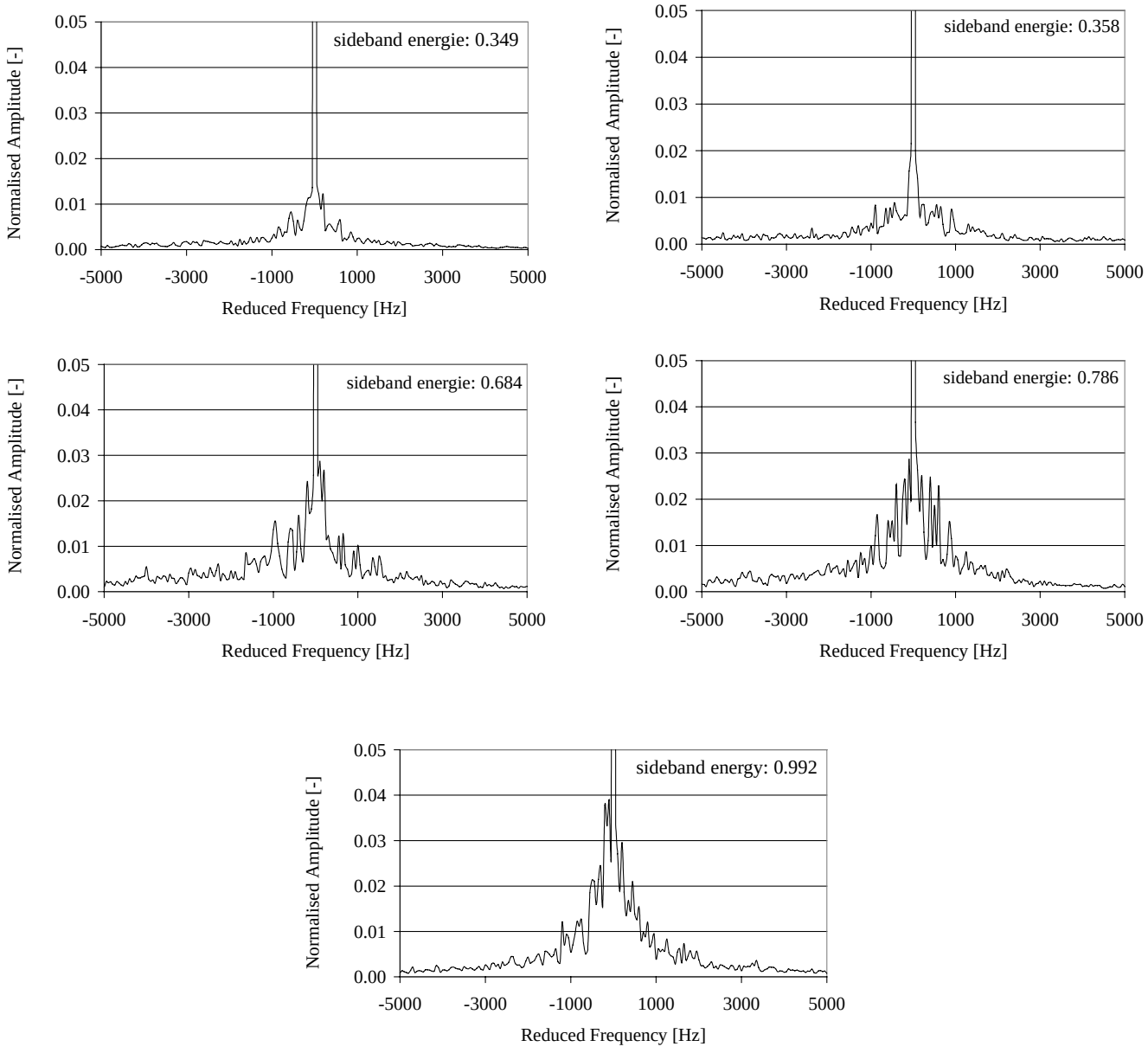

Fig. 9. Normalised and averaged spectra with corresponding values of the sideband energy for a selection of five fibre-cemented plates.

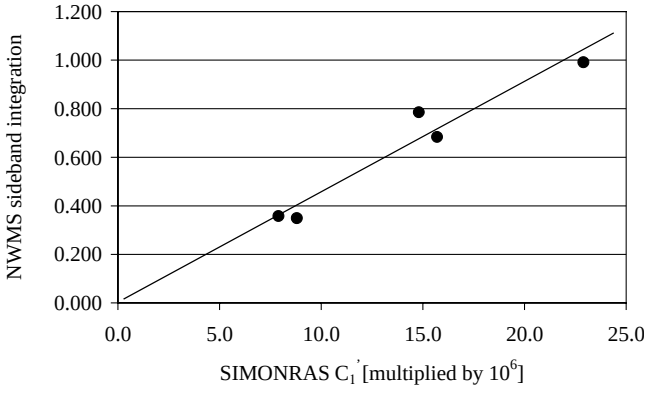

Fig. 10. Comparison between the sideband energy (NWMS measurement in impact mode) and the nonlinearity parameter C_1' (SIMONRAS experiment) for a selection of five plates.

the two cracked plates is primarily found in the top and bottom strips which contain microcracks that run along the fibre direction (perpendicular to the length of the strips). Plate P_2 shows a far larger increase in nonlinearity than P_1. Knowing that there are about as many cracks marked on P_2 as on P_1, this indicates that the edgecracks of P_2 are of a more severe nature than the cracks in P_1, or that the visual counting was not accurate. Note also that the increase of the nonlinearity of the edgestrips compared to the central strips (1–2 orders of magnitude) is far larger than the difference in SIMONRAS nonlinearity between a full size reference plate and a cracked one (only a factor 3–5). This is mainly due to the larger density of cracks per square unit in the edgestrips compared to the full size plates. Another remark is that the nonlinearity of

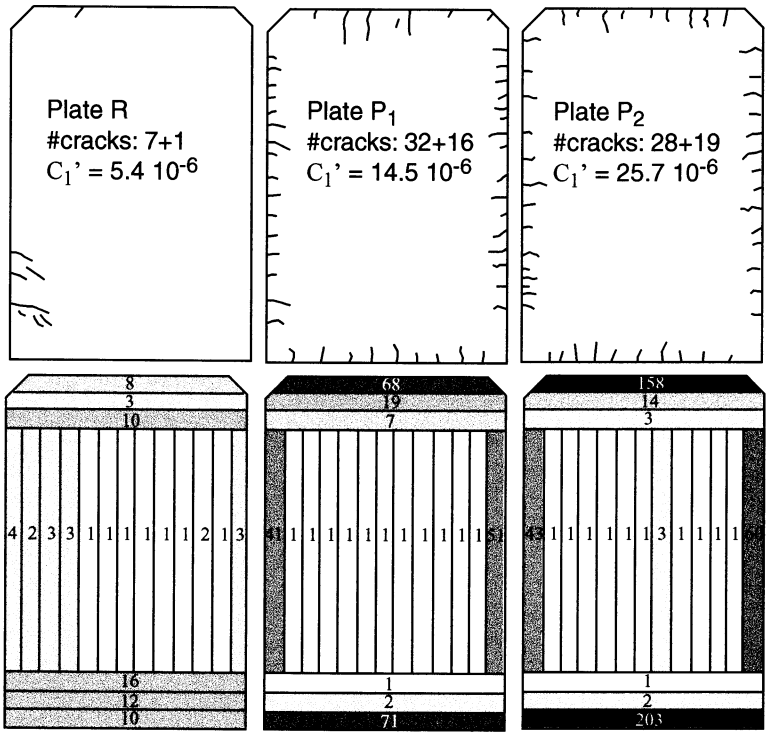

Fig. 11. Top row: location of the visually observed edgecracks for three fibre-cemented plates with corresponding crack-count number and SIMONRAS nonlinearity parameter C_1'. Bottom row: local relative values of the nonlinearity parameter (SIMONRAS experiment) after partitioning the above shown plates.

the vertical pieces (fibre direction along the length of the strip) is consistently lower than the nonlinearity of the lateral pieces (fibre direction perpendicular to the length). The anisotropy in the nonlinear behaviour can be explained by the fact that the formation of microcracks perpendicular to the fibres and the nonlinear activation of such microcracks and of other features in the bond system are counteracted by fibre bridging.

For the reference plate we note a far more continuous distribution of nonlinearity over the plate. The local increase of nonlinearity seems to match the cracked region which is indicated by visual inspection.

When inspecting the outermost lateral strips of the two cracked plates using X-ray radiography, we noticed that the second plate (with highest nonlinearity) showed several hairline cracks running along the edge of the strip (perpendicular to the edgecracks themselves). These cracks were not accounted for in visual inspection. This may be one of the reasons why the correlation between the crack-count and the nonlinearity turned out to be poor. It certainly suggests that one has to be careful in interpreting visual inspection results in terms of durability because cracks that are invisible for the unaided eye can be very important. In addition, it is obvious that crack-counts do not necessarily inform about the crack severity. Therefore, we believe that nonlinear techniques are more objective and also more reliable than any other visual or linear acoustic method with regard to the assessment of microdamage in a material.

4. Conclusions

We presented two recently developed nonlinear techniques which have a strong potential for microdamage detection in a wide variety of materials: SIMONRAS and NWMS. Nonlinear phenomena such as the amplitude dependence of the resonant frequency, the nonlinear attenuation, the distortion of a propagating wave by the creation of harmonics and the multiplication of waves of different frequencies, are extremely large in damaged materials when compared to an intact material. Because of the complex (i.e. nonlinear and hysteretic) compliance of cracks and flaws, the sensitivity of nonlinear methods to the detection of damage features is far greater than any linear acoustical methods.

We illustrated the latter statement with a couple of examples on thin slate beams subjected to cyclic and hydrothermal fatigue loading and on microcracked automobile components of irregular geometry. A complementary study on fibre-cemented plates was discussed to prove that both nonlinear techniques provide consistent results. In addition, we illustrated that a visual inspection method such as crack-counting can be a misleading technique for durability assessment. On the other hand, we showed that crackdensity is an important parameter in the sensitivity of nonlinear techniques. Certainly in cases of global damage, it is believed that nonlinear methods are superior in the investigation of the material's microcracking sensitivity.

Acknowledgements

This research has been financed by a research grant of the Research Council of the Catholic University of Leuven, Belgium, by the US Office of Basic Energy Research, Engineering and Geoscience (contract W-7405-ENG-36) and by a University Collaborative Research Program (921R) sponsored by The Institute of Geophysics and Planetary Physics at Los Alamos National Laboratory, NM, USA.

References

[1] Naugolnykh K, Ostrovsky L. Nonlinear wave processes in acoustics, Cambridge texts in applied mathematics. London: Cambridge University Press, 1998.
[2] Johnson PA, Guyer RA. The astonishing case of mesoscopic elastic nonlinearity. Phys Today 1999;April.
[3] Johnson PA, Rasolofosaon PNJ. Manifestation of nonlinear elasticity in rock: convincing evidence over large frequency and strain intervals from laboratory studies. Nonlinear Processes Geophys 1996;3:77–88.
[4] Nagy PB, Adler L. Acoustic nonlinearities in plastics. In: Thompson DO, Chimenti DE, editors. Review of progress in quantitative nondestructive evaluation, vol. 11. 1992. p. 2025–32.
[5] Van Den Abeele K, Johnson PA, Sutin AM. Nonlinear elastic wave spectroscopy (NEWS) techniques to discern material damage. Part I: nonlinear wave modulation spectroscopy. Res Nondest Eval 2000;12(1):17–30.
[6] Van Den Abeele K, Carmeliet J, TenCate JA, Johnson PA. Nonlinear elastic wave spectroscopy (NEWS) techniques to discern material damage. Part II: single mode nonlinear resonance acoustic spectroscopy. Res Nondest Eval 2000;12(1):31–42.
[7] Buck O, Morris WL, Richardson JN. Acoustic harmonic generation at unbonded interfaces and fatigue cracks. Appl Phys Lett 1978;33(5):371–3.
[8] Richardson M. Harmonic generation at an unbonded interface. I. Planar interface between semi-infinite elastic media. Int J Engng Sci 1979;17:73–5.
[9] Morris WL, Buck O, Inman RV. Acoustic harmonic generation due to fatigue damage in high-strength aluminum. J Appl Phys 1979;50(11):6737–41.
[10] Yost WT, Cantrell JH. Materials characterization using acoustic nonlinearity parameters and harmonic generation. In: Thompson DO, Chimenti DE, editors. Engineering materials, Review of progress in quantitative nondestructive evaluation, vol. 9B. New York: Plenum Press, 1990. p. 1669–76.
[11] Cantrell JH, Yost WT. Acoustic harmonic generation from fatigue — induces dislocation dipoles. Phil Mag A 1994;69:315–26.
[12] Nazarov VE, Ostrovskii LA, Soustova IA, Sutin AM. Anomaleous acoustic nonlinearity in metals. Sov Phys Acoust 1988;34:284–9.
[13] Nazarov VE, Sutin AM. Nonlinear elastic constants of solids with cracks. J Acoust Soc Am 1997;102(6):3349–54.
[14] Nagy PB, McGowan P, Adler L. Acoustic nonlinearities in adhesive joints. In: Thompson DO, Chimenti DE, editors. Review of progress in quantitative nondestructive evaluation, vol. 10B. New York: Plenum Press, 1990. p. 1685–92.
[15] Adler L, Nagy PB. Second order nonlinearities and their application in NDE. In: Thompson DO, Chimenti DE, editors. Review of progress in quantitative nondestructive evaluation, vol. 10B. New York: Plenum Press, 1991. p. 1813–20.
[16] Antonets VA, Donskoy DM, Sutin AM. Nonlinear vibro-diagnostics of flaws in multilayered structures. Mechanics Compos Mater 1986;15:934–7.
[17] Sutin AM, Declos C, Lenclud M. Investigations of the second harmonic generation due to cracks in large carbon electrodes. Proceedings of the 2nd Symposium on Acoustical and Vibratory Surveillance Methods and Diagnostic Techniques, Senlis, France, 1995. p. 725–35.
[18] Sutin AM, Nazarov VE. Nonlinear acoustic methods of crack diagnostics. Radiophys Quantum Electron 1995;38(3-4):109–20.
[19] Sutin AM, Donskoy DM. Vibro-acoustic modulation nondestructive evaluation technique. Proc SPIE 1998;3397:226–37.
[20] Johnson PA, Zinszner B, Rasolofosaon PNJ. Resonance and nonlinear elastic phenomena in rock. J Geophys Res 1996;11:553–64.
[21] Van Den Abeele K, TenCate JA. Acoustic characterization of nonlinear and hysteretic geomaterials: single mode nonlinear resonant ultrasound spectroscopy (SIMONRUS). Submitted for publication.
[22] Van Den Abeele K, Van De Velde K, Carmeliet J. Inferring the degradation of pultruded composites from dynamic nonlinear resonance measurements. Polym Compos 2000;August [in press].
[23] Van Den Abeele K, De Visscher J. Damage assessment in reinforced concrete using spectral and temporal nonlinear vibration techniques. Cem Concr Res 2000;30(9):1453–64.
[24] TenCate JA, Shankland TJ. Slow dynamics in the nonlinear elastic response of Berea sandstone. Geophys Res Lett 1996;23(21):3019–22.
[25] Guyer RA, McCall KR, Van Den Abeele K. Slow elastic dynamics in a resonant bar of rock. Geophys Res Lett 1998;25:1585–8.
[26] TenCate JA, Smith E, Guyer RA. Universal slow dynamics in granular solids. Phys Rev Lett 2000;85(5):1020–3.
[27] Nazarov VE, Ostrovsky LA, Soustova IA, Sutin AM. Nonlinear acoustics of micro-inhomogeneous media. Phys Earth Planet Interiors 1988;50:65–70.
[28] McCall KR, Guyer RA. Equation of state and wave propagation in hysteretic nonlinear elastic materials. J Geophys Res 1994;99:23,887–97.
[29] Guyer RA, McCall KR, Boitnott GN. Hysteresis, discrete memory and nonlinear wave propagation in rock: a new paradigm. Phys Rev Lett 1994;74:3491–4.
[30] McCall KR, Guyer RA. Hysteresis, discrete memory and nonlinear elastic wave propagation in rock: a new theoretical paradigm. Nonlinear Processes Geophys 1996;3:89–101.
[31] Nazarov VE. Propagation of a unipolar impulse in a medium with hysteretic nonlinearity. Akust Zh 1997;43:225–9 (English transl.: Acoust Phys 1997;43:192–5).
[32] Van Den Abeele K, Johnson PA, Guyer RA, McCall KR. On the quasi-analytic treatment of hysteretic nonlinear response in elastic wave propagation. J Acoust Soc Am 1997;101(4):1885–98.
[33] Gusev VE, Lauriks W, Thoen J. Dispersion of nonlinearity, nonlinear dispersion, and absorption of sound in micro-inhomogeneous materials. J Acoust Soc Am 1998;103(5):3216–26.
[34] Hamilton MF. Fundamentals and applications of nonlinear acoustics, in nonlinear wave propagation in mechanics — AMD-77. New York: The American Society of Mechanical Engineers, 1986.
[35] Landau LD, Lifshitz EM. Theory of elasticity. Tarrytown, NY: Pergamon, 1959.
[36] Van Den Abeele K. Elastic pulsed wave propagation in media with second- or higher-order nonlinearity. Part I: theoretical framework. J Acoust Soc Am 1996;99(6):3334–45.
[37] Stoker JJ. Nonlinear vibrations in mecahnical and electrical systems. New York: Interscience, 1950.
[38] Ungar EE, Kerwin EM. Loss factors of viscoelastic systems in terms of energy concepts. J Acoust Soc Am 1962;34(7):954–7.
[39] Smith DE, TenCate JA. Sensitive determination of nonlinear properties of Berea sandstone at low strains. Geophys Res Lett 2000;27:1985–8.